A hybrid cyt *c* maturation system enhances the bioelectrical performance of engineered *Escherichia coli* by improving the rate-limiting step

Author List:

Lin Su [1,2,3], Tatsuya Fukushima [3], Caroline M. Ajo-Franklin [2,3,4,5*]

Author Affiliations:

[1] State Key Laboratory of Bioelectronics, School of Biological Science and Medical Engineering, Southeast University, Nanjing 210018, China

[2] Department of BioSciences, Rice University, Houston, TX 77005, USA

[3] Molecular Foundry, Lawrence Berkeley National Laboratory, Berkeley, CA 94720, USA

[4] Molecular Biophysics and Integrated Biosciences Division, Lawrence Berkeley National Laboratory, Berkeley, CA 94720, USA

[5] Synthetic Biology Institute, Lawrence Berkeley National Laboratory, Berkeley, CA 94720, USA

* To whom correspondence should be addressed. Tel: 1-713-348-3497; Fax: 1-713-348-4790; Email: cajo-franklin@rice.edu

ABSTRACT

Bioelectronic devices can use electron flux to enable communication between biotic components and abiotic electrodes. We have modified *Escherichia coli* to electrically interact with electrodes by expressing the cytochrome *c* from *Shewanella oneidensis* MR-1. However, we observe inefficient electrical performance, which we hypothesize is due to the limited compatibility of the *E. coli* cytochrome *c* maturation (*ccm*) systems with MR-1 cyt *c*. Here we test whether the bioelectronic performance of *E. coli* can be improved by constructing hybrid *ccm* systems with parts from both *E. coli* and *S. oneidensis MR-1*. Our results show that the hybrid CcmH can increase cytochrome *c* expression and the stoichiometry of protein components also shifted. Electrochemical measurements show that the electron flux per cell increased 48% with the hybrid system. Additionally, the electrical response doubled with addition of exogenous flavin, which gives us a quantitative understanding of the bottleneck step in this electron conduit. These results demonstrate that this hybrid *ccm* system can enhance the bioelectrical performance of the cyt *c* expressing *Escherichia coli*, allowing to build more efficient bioelectronic devices.

KEYWORDS

Microbial electrochemistry, microbial fuel cell, bioelectronic sensor, synthetic biology, cytochrome *c* maturation

37 **1. INTRODUCTION**

38 The flow of electrons can transfer both energy and information between living and non-living
39 systems for bioelectronic and biosensing applications. Extracellular electron transfer (EET)
40 pathways (Shi et al., 2016) can electrically connect living microorganisms with electrochemical
41 cells, enabling applications such as power generation in microbial fuel cells (MFCs) (Gul and
42 Ahmad, 2019; Logan, 2009; Santoro et al., 2017; Slate et al., 2019) and environmental sensing in
43 bioelectronic sensing systems (Chouler et al., 2018; Wang et al., 2013; Zhou et al., 2017).
44 Engineering EET in native electroactive microorganisms, such as *Shewanella oneidensis* MR-1
45 (Cheng et al., 2020; Min et al., 2017; West et al., 2017), and non-native hosts, such as *Escherichia*
46 *coli (Jensen et al., 2016; Sturm-Richter et al., 2015)*, has expanded the range of potential
47 applications (Harris et al., 2017; Su and Ajo-Franklin, 2019). However, a fundamental limitation
48 in these bioelectronic systems is the low rate of EET, which causes these devices to have low
49 power output, low sensing sensitivity, and limited robustness. For example, expressing the EET
50 pathway from *Shewanella oneidensis* MR-1 into engineered *E. coli* only yields ~10% the current
51 produced by MR-1 (TerAvest et al., 2014).

52 Although the molecular structure of these EET pathways is increasingly well-understood, how
53 these complex proteins are biosynthesized is far less understood. The EET pathways (Mtr pathway)
54 in *Shewanella oneidensis* MR-1 is a group of multiheme cytochrome *c* (cyt *c*) proteins embedded
55 in the inner membrane (CymA), periplasm (ScyA, CctA, etc.), and outer membrane (MtrCAB
56 complex) (Clarke et al., 2011; Okamoto et al., 2011; Rosenbaum et al., 2012). Expressing these
57 cyt *c* requires the cytochrome *c* maturation (Ccm) system, which covalently ligates heme groups
58 to the apo-protein (Sanders et al., 2010; Verissimo et al., 2011). We and others have found that
59 expressing components of the Mtr pathway and the Ccm system enables *E. coli* to perform EET

60 (Jensen et al., 2016; Su et al., 2020; TerAvest et al., 2014). In the Ccm systems of Gram-negative
61 bacteria, CcmH is essential to the heme ligation process (Sanders et al., 2010), which includes
62 translocating heme groups, and formatting a thioether bond between the heme group and the apo
63 cyt *c*. We recently found that mutations in the C-terminal domain of CcmH can significantly
64 change the EET efficiency by changing the stoichiometry of the Mtr cyt *c (Su et al., 2020)*. This
65 finding suggested that optimizing the heme ligation process by redesigning CcmH could remodel
66 the stoichiometry of cyt *c* and enhance the bioelectrical performance of Mtr-expressing *E. coli*.

67 The role of the C-terminal domain of CcmH in cyt *c* maturation is disputed. Fabianek et al.
68 (Fabianek et al., 1999) and Robertson et al. (Robertson et al., 2008) demonstrated that a native
69 diheme cyt *c* (NapB) and a heterologous monoheme cyt *c* (Cyt c C550) can be matured in *E. coli*
70 lacking the C-terminal of CcmH. They contend that the C-terminal is not required for maturation
71 because of functional redundancy between the two domains of CcmH. In contrast, Zheng et al.
72 (Zheng et al., 2012) predicted the C-terminal of CcmH is a TRP (tetratricopeptide repeat) -like
73 domain which for recognition of apo-cyt *c* and predicts it is essential for cyt *c* expression. Our
74 previous results suggest the C-terminal of CcmH is essential in expressing multi-heme
75 heterologous cyt *c (Su et al., 2020)*, agreeing more closely with Zheng et al. (Zheng et al., 2012).

76 To determine if MR-1's ligation module is more efficient at maturing cyt *c*, here we constructed
77 a hybrid CcmH that uses protein domains from *E. coli* and *S. oneidensis* MR-1. We then explored
78 the effects on cyt *c* expression and EET efficiency to test if this hybrid CcmH could boost the
79 bioelectrical performance of Mtr-expressing *E. coli*.

80 **2. METHODS**

81 **2.1 Construction of *E. coli* strains with *ccm* variants**

82 We used Phusion DNA polymerase (NEB) for all the PCR amplification (please refer to
83 Supplementary Information for cloning procedures). We have listed all the primers, plasmids, and
84 strains we used in Table S1 and S2. We sequence verified all plasmids used and transformed them
85 into the *E. coli* C43(DE3) background (Lucigen) to construct all the strains.

86 **2.2 Cyt *c* expression and growth conditions for *E. coli* strains**

87 To express cyt *c*, we first grew all the *E. coli* strains directly from -80 °C glycerol stores in 5 mL
88 LB media with antibiotics (50 μg/mL kanamycin and 34 μg/mL chloramphenicol), incubated at
89 37 °C overnight with 250 rpm sharking. Then we inoculated cell cultures (1:100 v/v ratio) in 50
90 mL 2xYT media in foil-covered 250 mL flasks with the same antibiotic concentrations and 1 mM
91 δ-ALA (aminolevulinic acid), and grew these cultures at 37 °C with 250 rpm sharking. When the
92 cell OD_{600} reached between 0.5 to 0.6, we added 4 μM IPTG to induce the expression of cyt *c*,
93 followed by culturing at 30 °C with 250 rpm shaking overnight. Then we washed cells twice with
94 M9 minimal medium (BD). All the chemicals and media are from Sigma-Aldrich unless otherwise
95 noted.

96 **2.3 Redness screening of the *E. coli* strains with *ccm* variants**

97 We used redness screening for detecting the overall expression level of cyt *c*, as previously
98 described (Su et al., 2020). We first grew all the strains from -80 °C glycerol stores, then inoculated
99 cell cultures in 2xYT media with foil-covered flasks (see **section 2.2**). When the cell OD_{600} reached
100 between 0.5 to 0.6, we split the cell cultures into 96-well deep-well plates (Polypropylene 2.2 mL,
101 VWR), where each well contained 0.5 mL cell culture. We then induced the cells with a gradient
102 concentration of IPTG (0, 0.5, 1, 2, 4, 8, 16, 32, 62.5, 125, 250, and 500 μM). After overnight
103 incubation, we transferred the cell cultures into 96-well white round-bottom microplates (3789A,

104 Corning), and centrifuged to pellet the cells. After removing the media, we used a scanner to take
105 pictures of the plates and measured the redness of the cell pellets with a MATLAB image
106 processing program (Su et al., 2020).

107 **2.4 Enhanced chemiluminescence measurement of cyt *c* expression**

108 We used enhanced chemiluminescence (ECL) to detect the cyt *c* expression as previously
109 described (Su et al., 2020). In brief, we mixed 20 μL of 10 OD_{600} washed cells (described in **2.1**)
110 with an equal volume of Laemmli Sample Buffer (2x), and heated the mixture to 95°C for 15 min.
111 Then we loaded the samples and protein ladder (Precision Plus Protein WesternC Standards) into
112 an SDS-gel (4-20% Crit TGX Stain-Free Gel) to perform SDS-PAGE (160 V, 45 min). Next, we
113 transferred proteins from the SDS-gel onto the nitrocellulose membrane (Trans-Blot Turbo Midi
114 NC Transfer Packs) via the Trans-Blot Turbo Transfer System (Bio-Rad). We then used ECL kit
115 (Pierce Pico West Enhanced Chemiluminescence substrate, ThermoFisher) to perform the cyt *c*
116 detection assay. Finally, we used the FluorChem E system (ProteinSimple) to take the ECL images.
117 All the chemicals and supplies are from Bio-Rad unless otherwise indicated.

118 **2.5 Bioelectrochemical measurement**

119 We used two-chamber, three-electrode electrochemical reactors to perform the electrochemical
120 experiments as previously described (Su et al., 2020). The reactors contained three electrodes: a
121 working electrode (graphite felt, Alfa Aesar) and a reference electrode (CHI111, Ag/AgCl with 3
122 M KCl, CH Instruments) in the anodic chamber, and a counter electrode (titanium wire, Alfa Aesar)
123 in the cathodic chamber. We also used a cation exchange membrane (CMI-7000S, Membranes
124 International) to separate these two chambers. The electrolyte contained M9 minimal medium (BD)
125 and 50 mM D,L-lactate (Sigma-Aldrich). During the test, we continuously purged the anodic

126 chamber with N_2 gas to maintain anaerobic conditions, and we kept the temperature at 30 °C by
127 placing all the reactors in an incubator. We used a potentiostat (VSP-300, Bio-Logic Science
128 Instruments) to perform all the electrochemical measurements. We set the applied potential at 0.2
129 V versus the reference electrode to conduct chronoamperometry, and the electrical current
130 (averaged at every 36 s) is reported as a function of the geometric surface area of the working
131 electrode. For the differential pulse voltammetry (DPV) measurement (Xu et al., 2016), we
132 scanned the potential from -0.4 V to 0.2 V versus the reference electrode, with the pulse height set
133 to 50 mV, pulse width set to 500 ms, step height set to 1.0 mV, and step time set to 1000 ms.

134 **3. RESULTS AND DISCUSSION**

135 **3.1 Design and construction of a hybrid cyt *c* maturation operon in *Escherichia coli***

136 To test our hypothesis that MR-1's ligation module is more efficient at maturing MR-1 cyt *c* than
137 *E. coli*'s ligation module, we made a series of modifications to the *ccmH* gene in the plasmid which
138 carries the *ccm* operon from *E. coli* (Figure 1). To test the effect of altering the entire ligation
139 module, we replaced *ccmH* from *E. coli* with *ccmHI* from MR-1, creating the *ccmHI* plasmid. To
140 test the impact of replacing only the apo cyt *c* binding component, we fused the N-terminal region
141 of the *E. coli ccmH* with the C terminal region of MR-1 *ccmI*, notated as the hybrid *ccmH* plasmid.
142 As a control, we also made a $ccmH^N$ plasmid from the hybrid *ccmH* plasmid, in which the C-
143 terminal domain of *S. oneidensis* CcmI was removed. We then co-transformed the *ccm*, *ccmHI*,
144 hybrid *ccmH* and $ccmH^N$ plasmids with a separate plasmid that expresses *cymAmtrCAB* from MR-
145 1 (Figure S1) into *E. coli* C43(DE3) to create the wildtype *ccm*, *ccmHI*, $ccmH^N$, and hybrid *ccmH*
146 strains. We also constructed a strain with the pACYC184 empty vector and *cymAmtrCAB* plasmid,
147 dubbed the 'no *ccm'* strain, as a negative control.

148 **3.2 The hybrid *ccm* system can increase cyt *c* abundance in *E. coli***

149 To test if these *ccm* variants can mature and change the cyt *c* expression level, we first examined
150 the cyt *c* expression of these *E. coli* strains with a redness assay (Su et al., 2020) across different
151 IPTG inducing levels (Figure 2), i.e., different promoter strength (Goldbeck et al., 2013). The
152 redness value, which indirectly measures the cyt *c* abundance per cell, peaked at the relative
153 promoter strength region around 0.1 intensity (arb. units) for all the strains with a *ccm* plasmid. As
154 expected, the no *ccm* strain has the lowest redness value because it cannot mature cyt *c,* and the
155 wildtype *ccm* has a high redness value, consistent with its ability to mature cyt *c*. Compared to the
156 wildtype *ccm* strain, the redness value of *ccmHI* strain decreased by ~40% (0.15 ± 0.003 in *ccmHI*
157 vs. 0.25 ± 0.003 in wildtype). This decrease in cyt *c* expression might be due to a poor ability of
158 the *E. coli* and MR-1 proteins to form a functional complex (Zheng et al., 2012). In contrast, the
159 hybrid *ccmH* strain has redness value (0.27 ± 0.002) that is 8% greater than the wildtype *ccm*,
160 indicating that this strain can mature cyt *c* slightly better than the wildtype. Increased cyt c
161 expression in hybrid *ccmH* strain shows the C terminal region of CcmI from MR-1 can functionally
162 replace the C terminal region of *E. coli ccmH*. Overall, these data show that the hybrid *ccm* system
163 can increase cyt *c* abundance in *E. coli*, which potentially may increase its EET efficiency.

164 **3.3 The hybrid *ccm* system changes Mtr cyt *c* stoichiometry**

165 To further investigate how the hybrid *ccm* system alters the expression of cyt *c* in the Mtr pathway,
166 we used enhanced chemiluminescence (ECL) to characterize the abundance of CymA, MtrC, and
167 MtrA in hybrid *ccmH* strain, wildtype *ccm* strain, and no *ccm* strain (**Figure S2**). These strains
168 were all induced at 0.068 relative promoter strength since the hybrid *ccm* strain has the highest cyt
169 *c* expression at this induction (Figure 2). As expected, there was no detectable amount of cyt *c* in

170 the no *ccm* strain (**Figure S2**). While the MtrC abundance was very similar, the abundance of
171 MtrA decreased ~15%, and CymA increased ~60% in the hybrid *ccm* strain relative to the wildtype
172 *ccm* strain (Figure 3). These data show that the hybrid *ccm* system increases the overall cyt *c*
173 abundance by increasing the maturation of CymA.

174 **3.4 The hybrid *ccm* system increases the current generation of Mtr-expressing *E. coli***

175 Altering the stoichiometry of Mtr cyt *c* in *E. coli* can negatively or positively affect its
176 bioelectrochemical performance (Su et al., 2020). To probe if the increase of CymA expression in
177 hybrid *ccmH* strain will also enhance its bioelectrical performance, we measured the current
178 generation (Figure 4) by the wildtype *ccm*, hybrid *ccmH*, $ccmH^N$ strains in three-electrode
179 electrochemistry bioreactors. The wildtype *ccm* strain produced 11.47 ± 0.19 mA/m^2, in line with
180 our previous observations (Su et al., 2020). The hybrid *ccmH* produced 25.32 ± 3.61mA/m^2, a 121%
181 increase in current over the wildtype *ccm*. The $ccmH^N$ produced only 3.42 ± 0.44 mA/m^2, about a
182 70% decrease relative to the wildtype *ccm*, similar to the no *mtr* strain previously reported
183 (TerAvest et al., 2014). Thus, we conclude that the hybrid *ccmH* strain matures more CymA and
184 produces higher current than the *E. coli ccm* system.

185 To probe the mechanism underlying the increase in current production by the hybrid *ccmH* strain,
186 we performed differential pulse voltammetry (DPV) (Figure 5) after strains reached the steady-
187 state current generation after 90 h chronoamperometry testing. We observed a single anodic peak
188 at redox potential (E_p) of +51 mV_{SHE} in all three strains, which has been previously assigned to the
189 MtrCAB complex *(Okamoto et al., 2013)*. This observation confirms that all three strains use the
190 MtrCAB conduit for the current production. The peak height in hybrid *ccmH* strain reached 8.31
191 μA, about 118% higher than the 3.82 μA in wildtype *ccm* strain, while in the $ccmH^N$ strain, it was

192 only 0.09 μA, about 2% of the wildtype. The ratio of the peak height for the hybrid *ccm* strain
193 relative to the wildtype *ccm* strain (2.18) closely mirrors the ratio of steady-state current for these
194 strains (2.21), indicating the increase in steady-state current arises from an increase in the flux of
195 electrons through the MtrCAB complex. Thus, the hybrid *ccm* strain produces more current by
196 more effectively maturing CymA, boosting its relative abundance, and increasing the electron flux
197 through the MtrCAB conduit.

198 **3.5 Hybrid *ccmH* strain produces more current per cell via both direct and indirect EET**

199 While DPV confirms that the increase in electron flux through the Mtr pathway increases the
200 current density, this increased flux could arise from an increase in the current per cell, an increase
201 in the number of viable cells, or an increase in both. To distinguish between these possibilities, we
202 measured both the current production and the number of viable cells using colony-forming unit
203 counting in the $ccmH^N$, hybrid *ccm*, and wildtype *ccm* strains (Figure 6A). The $ccmH^N$ strain
204 produced near baseline current on a per cell basis (1.0 ± 0.005 fA·cell^{-1}), as expected. Interestingly,
205 the hybrid *ccmH* strains produced ~50% more current per cell than the wildtype *ccm* (12.3 ± 0.3
206 fA·cell^{-1} versus 8.3 ± 0.4 fA·cell^{-1}). These data confirm that the hybrid *ccmH* strain produces more
207 current at the single-cell level by direct EET.

208 In addition to direct EET, MR-1 (Brutinel and Gralnick, 2012; Coursolle et al., 2010) as a bound
209 cofactor (Edwards et al., 2015; Okamoto et al., 2014)or as a soluble mediator (Kotloski and
210 Gralnick, 2013). To test if the hybrid *ccmH* strain can also utilize flavin for EET, we added
211 exogenous flavins and measured the current density per cell. The addition of riboflavin to the
212 $ccmH^N$ strain resulted in a meager current increase (0.02 ± 0.004 fA·cell^{-1}·μM^{-1}). As expected, the
213 current produced by both the wildtype *ccm* and hybrid *ccm* linearly increased with the exogenous

214 flavin concentration (Figure 6A). However, the hybrid *ccm* strain produced significantly more
215 current per μM exogenous flavin (0.32 ± 0.06 fA·cell^{-1}· μM^{-1}) than the wildtype *ccm* (0.16 ± 0.01
216 fA·cell^{-1}·μM^{-1}) (Figure 6A). These data indicate that the hybrid *ccm* strain produces more current
217 at the single-cell level via a flavin-mediated EET as well as a direct EET mechanism.

218 **3.6 Direct and flavin-mediated EET in the hybrid *ccmH* strain is limited by CymA**

219 Our data suggest that CymA amount limits electron flux and that the hybrid *ccm* strain
220 achieves higher current by enabling a greater electron flux from CymA into the same direct and
221 indirect EET routes found in the wildtype *ccm* strain. To quantitatively test these hypotheses, we
222 developed a quantitative model that relates EET in the hybrid *ccm* strain to EET in the wildtype
223 *ccm* strain and then tested whether this model could explain the current per cell measurement in
224 the hybrid *ccm* strain (Figure 6).

225 Explicitly, we modeled the overall EET current per cell (I_{strain}) as the sum of the direct EET
226 via Mtr conduit (I_{Mtr}) and flavin-mediated EET (I_{flavin}) (Figure 6B). We describe the flavin-
227 mediated EET as the product of the flavin concentration ($[flavin]$) and a constant of
228 proportionality (k_{strain}), (**Equation 1**):

229 $$I_{strain} = I_{strain,Mtr} + I_{strain,flavin} = I_{strain,Mtr} + k_{strain}[flavin] \quad (1)$$

230 Assuming the concentration of CymA is rate-limiting in our system (Figure 3), both I_{Mtr} and I_{flavin}
231 should be dependent on the CymA concentration (**Equation 2**).

232 $$I_{strain,Mtr} = a[CymA]_{strain};\ I_{strain,flavin} = b[CymA]_{strain}k_{strain}[flavin] \quad (2)$$

233 By substituting and rearranging, we can then calculate EET current in the hybrid *ccmH* strain
234 (I_{hybrid}) as a ratio of the CymA concentration in the two strains and the current in the wildtype *ccm*
235 strain ($I_{WT,Mtr}$) with the equation below (**Equation 3**).

236 $$I_{hybrid} = \frac{[CymA]_{hybrid}}{[CymA]_{WT}} I_{WT,Mtr} + \frac{[CymA]_{hybrid}}{[CymA]_{WT}} k_{WT}[flavin] \quad (3)$$

237 Thus, both the intercept and slope of the best-fit line for the hybrid *ccm* strain should be equal to
238 the intercept and slope best-fit line of the wildtype *ccm* strain times the ratio of CymA
239 concentration in these two strains.

240 Using the experimentally-determined values of $I_{WT,Mtr}$ (8.3 ± 0.4 fA·cell^{-1}), k_{WT} (0.16 ± 0.01
241 fA·cell^{-1}·μM^{-1}), and $[CymA]_{hybrid}/[CymA]_{WT}$ = 1.6, we can predict the values of I_{hybrid} and compare
242 it to our experimentally-determined values (Figure 6A). Both the predicted $I_{hybrid, Mtr}$ and $I_{hybrid, flavin}$
243 values, 13.28±0.64 fA·cell^{-1} and 0.26 ± 0.02 fA·cell^{-1}·μM^{-1}, respectively, are quite close to our
244 observation of the direct EET (12.3 ± 0.3 fA·cell^{-1}) and mediated EET (0.32 ± 0.06 fA·cell^{-1}·μM^{-}
245 ^{1}) in hybrid *ccmH* strain. This result provides strong evidence that the hybrid *ccmH* strain's
246 improved bioelectrochemical performance arises mainly from the CymA expression increase and
247 underscores the importance of CymA in both direct EET and indirect EET.

248 **4. DISCUSSION**

249 In this study, we have shown that the C-terminal region of CcmH can be complemented by the
250 homologous region of CcmI from *S. oneidensis* MR-1, which increases the bioelectronic
251 performance of Mtr-expressing *E. coli*. We found that the hybrid *ccm* can increase the overall cyt
252 *c* expression (Figure 2), with a preferred 60% increase in CymA expression (Figure 3). This
253 increase in CymA expression led to a 48% more EET current per bacterium and doubled the

254 electrical response to exogenous flavin (Figure 5), consistent with CymA being rate limiting in
255 EET. In the following, we discuss how these findings impact the development of biofuel cells and
256 biosensors.

257 First, our data show that the C-terminal region of CcmH is essential for cyt *c*-based EET.
258 *Shewanella* and *Geobacter* species are the dominant organisms used for EET applications, such as
259 MFCs. These microorganisms express a significant amount of cyt *c* to perform EET (Meyer et al.,
260 2004; Shi et al., 2009). As a result, there are increasing efforts focused on genetically introducing
261 cyt *c* to make new organisms capable of EET ((Schuergers et al., 2017; Sekar et al., 2016;
262 Thirumurthy and Jones, 2020), overexpressing cyt *c* to understand the structural basis of EET (M.
263 Edwards et al., 2019; M. J. Edwards et al., 2019; Wang et al., 2019), and making cyt *c* -based
264 conductive biomaterials for bioelectrical applications (Liu et al., 2020; Sun et al., 2018).
265 Understanding how cyt *c* mature can provide guidance on manipulating cyt *c* expression, which
266 will assist both fundamental studies and these applied efforts to increase the bioelectrical
267 performance of MFCs.

268 Second, we found that the hybrid *ccmH* strain generates higher electrical signals using both Mtr
269 and flavin-mediated EET. Increasing the EET efficiency of Mtr-expressing *E. coli* is of particular
270 interest for biosensing because it can increase the signal-to-noise ratio, enabling higher sensitivity
271 detection. In recent years, much progress has been made in engineering the electrical
272 communication between bacteria and electrodes, such as responding to specific chemicals using
273 chemical-sensitive promoters (Golitsch et al., 2013; Webster et al., 2014; Yang et al., 2018),
274 miniaturized reactors with optimized structure design (Zhou et al., 2017), and modified material-
275 bacteria interface (Zajdel et al., 2018). Enhancing the bioelectrical performance of Mtr-expression
276 *E. coli* offers a reliable chassis in biosensing applications.

277 Last, the cyt *c* stoichiometry shifts to more abundant in CymA, which guides us on how to build
278 a more efficient EET conduit for bioelectrical sensing. Our analysis of modeling the current
279 generation in hybrid *ccmH* strain, with and without exogenous flavin, together with the fact that
280 CymA can only carry 40% (fewer heme groups per protein) as many electrons as MtrA or MtrC,
281 highly suggests that electron transfer through CymA is a bottleneck for EET in the Mtr-expression
282 *E. coli*. Future work will focus on increasing the electron flux between menaquinone and the
283 MtrCAB complex to overcome this rate-limiting step. Also, the electrical response we observed
284 which is linear to both CymA amount and flavin concentration, could expand the application
285 scenarios such as building an "AND" gate with dual inputs.

286 **5. CONCLUSIONS**

287 In summary, a hybrid *ccm* system altered the stoichiometry of the expressed cyt *c,* thus
288 accelerating the rate limiting step in EET and enhancing the bioelectronic performance of *E. coli*.
289 Our results suggest that increasing the electron flux from menaquinone to MtrCAB complex could
290 further enhance the bioelectrical performance of engineered *E. coli*. More broadly, our work
291 provides a new strategy to express cyt *c* that underlie microbial bioelectronics and opens new
292 possibilities for engineering more sophisticated and sensitive biosensors.

293 **SUPPLEMENTARY DATA**

294 The Supporting Information is available online.

295 **ABBREVIATIONS**

296 cyt *c*, EET, ccm, MFC.

AUTHOR CONTRIBUTIONS

L.S. contributed to strains construction, design of the study, conducting experiments, analysis of the data, and writing of the manuscript. T.F. contributed to strain construction, design of the study, conducting experiments, analysis of the data, review and editing the manuscript. C.M.A-F. contributed to the design of the study, analysis of the data, and writing of the manuscript.

ACKNOWLEDGMENT

We thank Dr. Shuai Xu and Prof. Mohamed Y. El-Naggar, the University of Southern California for discussions on the DPV experiments. Work at the Molecular Foundry was supported by the Office of Science, Office of Basic Energy Sciences, of the U.S. Department of Energy [DE-AC02-05CH11231]. This work was supported by the Office of Naval Research, [N0001418IP00037]; and the China Scholarship Council [201606090098 to L.S.].

309 **REFERENCES**

310 Brutinel, E.D., Gralnick, J.A., 2012. Shuttling happens: soluble flavin mediators of extracellular electron
311 transfer in Shewanella. Appl. Microbiol. Biotechnol. 93, 41–48. https://doi.org/10.1007/s00253-011-
312 3653-0

313 Cheng, Z., Xiong, J., Min, D., Cheng, L., Liu, D., Li, W., Jin, F., Yang, M., Yu, H., 2020. Promoting
314 bidirectional extracellular electron transfer of Shewanella oneidensis MR-1 for hexavalent chromium
315 reduction via elevating intracellular cAMP level. Biotechnol. Bioeng.
316 https://doi.org/10.1002/bit.27305

317 Chouler, J., Cruz-Izquierdo, Á., Rengaraj, S., Scott, J.L., Di Lorenzo, M., 2018. A screen-printed paper
318 microbial fuel cell biosensor for detection of toxic compounds in water. Biosens. Bioelectron. 102,
319 49–56. https://doi.org/10.1016/j.bios.2017.11.018

320 Clarke, T.A., Edwards, M.J., Gates, A.J., Hall, A., White, G.F., Bradley, J., Reardon, C.L., Shi, L.,
321 Beliaev, A.S., Marshall, M.J., Wang, Z., Watmough, N.J., Fredrickson, J.K., Zachara, J.M., Butt,
322 J.N., Richardson, D.J., 2011. Structure of a bacterial cell surface decaheme electron conduit. Proc.
323 Natl. Acad. Sci. U. S. A. 108, 9384–9389. https://doi.org/10.1073/pnas.1017200108

324 Coursolle, D., Baron, D.B., Bond, D.R., Gralnick, J.A., 2010. The Mtr respiratory pathway is essential for
325 reducing flavins and electrodes in Shewanella oneidensis. J. Bacteriol. 192, 467–474.
326 https://doi.org/10.1128/JB.00925-09

327 Edwards, M.J., Richardson, D.J., Paquete, C.M., Clarke, T.A., 2019. Role of multiheme cytochromes
328 involved in extracellular anaerobic respiration in bacteria. Protein Sci.
329 https://doi.org/10.1002/pro.3787

330 Edwards, M.J., White, G.F., Norman, M., Tome-Fernandez, A., Ainsworth, E., Shi, L., Fredrickson, J.K.,
331 Zachara, J.M., Butt, J.N., Richardson, D.J., Clarke, T.A., 2015. Redox Linked Flavin Sites in
332 Extracellular Decaheme Proteins Involved in Microbe-Mineral Electron Transfer. Sci. Rep. 5, 11677.
333 https://doi.org/10.1038/srep11677

334 Edwards, M., White, G., Butt, J., Richardson, D.J., Clarke, T.A., 2019. The Structure of a Biological
335 Insulated Transmembrane Molecular Wire. https://doi.org/10.2139/ssrn.3445677
336 Fabianek, R.A., Hofer, T., Thöny-Meyer, L., 1999. Characterization of the Escherichia coli CcmH protein
337 reveals new insights into the redox pathway required for cytochrome c maturation. Arch. Microbiol.
338 171, 92–100. https://doi.org/10.1007/s002030050683
339 Fourmond, V., Hoke, K., Heering, H.A., Baffert, C., Leroux, F., Bertrand, P., Léger, C., 2009. SOAS: a
340 free program to analyze electrochemical data and other one-dimensional signals.
341 Bioelectrochemistry 76, 141–147. https://doi.org/10.1016/j.bioelechem.2009.02.010
342 Goldbeck, C.P., Jensen, H.M., TerAvest, M.A., Beedle, N., Appling, Y., Hepler, M., Cambray, G.,
343 Mutalik, V., Angenent, L.T., Ajo-Franklin, C.M., 2013. Tuning promoter strengths for improved
344 synthesis and function of electron conduits in Escherichia coli. ACS Synth. Biol. 2, 150–159.
345 https://doi.org/10.1021/sb300119v
346 Golitsch, F., Bücking, C., Gescher, J., 2013. Proof of principle for an engineered microbial biosensor
347 based on Shewanella oneidensis outer membrane protein complexes. Biosens. Bioelectron. 47, 285–
348 291. https://doi.org/10.1016/j.bios.2013.03.010
349 Gul, M.M., Ahmad, K.S., 2019. Bioelectrochemical systems: Sustainable bio-energy powerhouses.
350 Biosens. Bioelectron. 142, 111576. https://doi.org/10.1016/j.bios.2019.111576
351 Harris, H.W., Sánchez-Andrea, I., McLean, J.S., Salas, E.C., Tran, W., El-Naggar, M.Y., Nealson, K.H.,
352 2017. Redox Sensing within the Genus Shewanella. Front. Microbiol. 8, 2568.
353 https://doi.org/10.3389/fmicb.2017.02568
354 Jensen, H.M., TerAvest, M.A., Kokish, M.G., Ajo-Franklin, C.M., 2016. CymA and Exogenous Flavins
355 Improve Extracellular Electron Transfer and Couple It to Cell Growth in Mtr-Expressing Escherichia
356 coli. ACS Synth. Biol. 5, 679–688. https://doi.org/10.1021/acssynbio.5b00279
357 Kotloski, N.J., Gralnick, J.A., 2013. Flavin Electron Shuttles Dominate Extracellular Electron Transfer by
358 Shewanella oneidensis. mBio. https://doi.org/10.1128/mbio.00553-12
359 Liu, X., Gao, H., Ward, J.E., Liu, X., Yin, B., Fu, T., Chen, J., Lovley, D.R., Yao, J., 2020. Power

generation from ambient humidity using protein nanowires. Nature. https://doi.org/10.1038/s41586-020-2010-9

Logan, B.E., 2009. Exoelectrogenic bacteria that power microbial fuel cells. Nature Reviews Microbiology. https://doi.org/10.1038/nrmicro2113

Meyer, T.E., Tsapin, A.I., Vandenberghe, I., de Smet, L., Frishman, D., Nealson, K.H., Cusanovich, M.A., van Beeumen, J.J., 2004. Identification of 42 possible cytochrome C genes in the Shewanella oneidensis genome and characterization of six soluble cytochromes. OMICS 8, 57–77. https://doi.org/10.1089/153623104773547499

Min, D., Cheng, L., Zhang, F., Huang, X.-N., Li, D.-B., Liu, D.-F., Lau, T.-C., Mu, Y., Yu, H.-Q., 2017. Enhancing Extracellular Electron Transfer of Shewanella oneidensis MR-1 through Coupling Improved Flavin Synthesis and Metal-Reducing Conduit for Pollutant Degradation. Environmental Science & Technology. https://doi.org/10.1021/acs.est.6b04640

Okamoto, A., Hashimoto, K., Nealson, K.H., Nakamura, R., 2013. Rate enhancement of bacterial extracellular electron transport involves bound flavin semiquinones. Proc. Natl. Acad. Sci. U. S. A. 110, 7856–7861. https://doi.org/10.1073/pnas.1220823110

Okamoto, A., Nakamura, R., Hashimoto, K., 2011. In-vivo identification of direct electron transfer from Shewanella oneidensis MR-1 to electrodes via outer-membrane OmcA–MtrCAB protein complexes. Electrochim. Acta 56, 5526–5531. https://doi.org/10.1016/j.electacta.2011.03.076

Okamoto, A., Nakamura, R., Nealson, K.H., Hashimoto, K., 2014. Bound Flavin Model Suggests Similar Electron-Transfer Mechanisms in Shewanella and Geobacter. CHEMELECTROCHEM 1, 1808–1812. https://doi.org/10.1002/celc.201402151

Robertson, I.B., Stevens, J.M., Ferguson, S.J., 2008. Dispensable residues in the active site of the cytochrome c biogenesis protein CcmH. FEBS Lett. 582, 3067–3072. https://doi.org/10.1016/j.febslet.2008.07.052

Rosenbaum, M.A., Bar, H.Y., Beg, Q.K., Segrè, D., Booth, J., Cotta, M.A., Angenent, L.T., 2012. Transcriptional analysis of Shewanella oneidensis MR-1 with an electrode compared to Fe(III)citrate

386 or oxygen as terminal electron acceptor. PLoS One 7, e30827.
387 https://doi.org/10.1371/journal.pone.0030827
388 Sanders, C., Turkarslan, S., Lee, D.-W., Daldal, F., 2010. Cytochrome c biogenesis: the Ccm system.
389 Trends Microbiol. 18, 266–274. https://doi.org/10.1016/j.tim.2010.03.006
390 Santoro, C., Arbizzani, C., Erable, B., Ieropoulos, I., 2017. Microbial fuel cells: From fundamentals to
391 applications. A review. J. Power Sources 356, 225–244.
392 https://doi.org/10.1016/j.jpowsour.2017.03.109
393 Schuergers, N., Werlang, C., Ajo-Franklin, C.M., Boghossian, A.A., 2017. A Synthetic Biology
394 Approach to Engineering Living Photovoltaics. Energy Environ. Sci. 10, 1102–1115.
395 https://doi.org/10.1039/C7EE00282C
396 Sekar, N., Jain, R., Yan, Y., Ramasamy, R.P., 2016. Enhanced photo-bioelectrochemical energy
397 conversion by genetically engineered cyanobacteria. Biotechnol. Bioeng. 113, 675–679.
398 https://doi.org/10.1002/bit.25829
399 Shi, L., Dong, H., Reguera, G., Beyenal, H., Lu, A., Liu, J., Yu, H.-Q., Fredrickson, J.K., 2016.
400 Extracellular electron transfer mechanisms between microorganisms and minerals. Nat. Rev.
401 Microbiol. 14, 651–662. https://doi.org/10.1038/nrmicro.2016.93
402 Shi, L., Richardson, D.J., Wang, Z., Kerisit, S.N., Rosso, K.M., Zachara, J.M., Fredrickson, J.K., 2009.
403 The roles of outer membrane cytochromes of Shewanella and Geobacter in extracellular electron
404 transfer. Environ. Microbiol. Rep. 1, 220–227. https://doi.org/10.1111/j.1758-2229.2009.00035.x
405 Slate, A.J., Whitehead, K.A., Brownson, D.A.C., Banks, C.E., 2019. Microbial fuel cells: An overview of
406 current technology. Renewable Sustainable Energy Rev. 101, 60–81.
407 https://doi.org/10.1016/j.rser.2018.09.044
408 Sturm-Richter, K., Golitsch, F., Sturm, G., Kipf, E., Dittrich, A., Beblawy, S., Kerzenmacher, S.,
409 Gescher, J., 2015. Unbalanced fermentation of glycerol in Escherichia coli via heterologous
410 production of an electron transport chain and electrode interaction in microbial electrochemical cells.
411 Bioresour. Technol. 186, 89–96. https://doi.org/10.1016/j.biortech.2015.02.116

412 Su, L., Ajo-Franklin, C.M., 2019. Reaching full potential: bioelectrochemical systems for storing
413 renewable energy in chemical bonds. Curr. Opin. Biotechnol. 57, 66–72.
414 https://doi.org/10.1016/j.copbio.2019.01.018
415 Su, L., Fukushima, T., Prior, A., Baruch, M., Zajdel, T.J., Ajo-Franklin, C.M., 2020. Modifying
416 cytochrome c maturation can increase bioelectronic performance of engineered Escherichia coli.
417 ACS Synth. Biol. 9, 115–124. https://doi.org/10.1021/acssynbio.9b00379
418 Sun, Y.-L., Tang, H.-Y., Ribbe, A., Duzhko, V., Woodard, T.L., Ward, J.E., Bai, Y., Nevin, K.P.,
419 Nonnenmann, S.S., Russell, T., Emrick, T., Lovley, D.R., 2018. Conductive Composite Materials
420 Fabricated from Microbially Produced Protein Nanowires. Small 14, e1802624.
421 https://doi.org/10.1002/smll.201802624
422 TerAvest, M.A., Zajdel, T.J., Ajo-Franklin, C.M., 2014. The Mtr pathway of shewanella oneidensis MR-1
423 couples substrate utilization to current production in escherichia coli. ChemElectroChem 1, 1874–
424 1879.
425 Thirumurthy, M.A., Jones, A.K., 2020. Geobacter cytochrome OmcZs binds riboflavin: implications for
426 extracellular electron transfer. Nanotechnology 31, 124001. https://doi.org/10.1088/1361-
427 6528/ab5de6
428 Verissimo, A.F., Yang, H., Wu, X., Sanders, C., Daldal, F., 2011. CcmI subunit of CcmFHI heme ligation
429 complex functions as an apocytochrome c chaperone during c-type cytochrome maturation. J. Biol.
430 Chem. 286, 40452–40463. https://doi.org/10.1074/jbc.M111.277764
431 Wang, F., Gu, Y., O'Brien, J.P., Yi, S.M., Yalcin, S.E., Srikanth, V., Shen, C., Vu, D., Ing, N.L.,
432 Hochbaum, A.I., Egelman, E.H., Malvankar, N.S., 2019. Structure of Microbial Nanowires Reveals
433 Stacked Hemes that Transport Electrons over Micrometers. Cell 177, 361–369.e10.
434 https://doi.org/10.1016/j.cell.2019.03.029
435 Wang, X., Gao, N., Zhou, Q., 2013. Concentration responses of toxicity sensor with Shewanella
436 oneidensis MR-1 growing in bioelectrochemical systems. Biosens. Bioelectron. 43, 264–267.
437 https://doi.org/10.1016/j.bios.2012.12.029

438 Webster, D.P., TerAvest, M.A., Doud, D.F.R., Chakravorty, A., Holmes, E.C., Radens, C.M., Sureka, S.,
439 Gralnick, J.A., Angenent, L.T., 2014. An arsenic-specific biosensor with genetically engineered
440 Shewanella oneidensis in a bioelectrochemical system. Biosens. Bioelectron. 62, 320–324.
441 https://doi.org/10.1016/j.bios.2014.07.003
442 West, E.A., Jain, A., Gralnick, J.A., 2017. Engineering a Native Inducible Expression System in
443 Shewanella oneidensis to Control Extracellular Electron Transfer. ACS Synth. Biol. 6, 1627–1634.
444 https://doi.org/10.1021/acssynbio.6b00349
445 Xu, S., Jangir, Y., El-Naggar, M.Y., 2016. Disentangling the roles of free and cytochrome-bound flavins
446 in extracellular electron transport from Shewanella oneidensis MR-1. Electrochim. Acta 198, 49–55.
447 https://doi.org/10.1016/j.electacta.2016.03.074
448 Yang, Y., Zhou, H., Mei, X., Liu, B., Xing, D., 2018. Dual-Edged Character of Quorum Sensing
449 Signaling Molecules in Microbial Extracellular Electron Transfer. Front. Microbiol. 9, 1924.
450 https://doi.org/10.3389/fmicb.2018.01924
451 Zajdel, T.J., Baruch, M., Méhes, G., Stavrinidou, E., Berggren, M., Maharbiz, M.M., Simon, D.T., Ajo-
452 Franklin, C.M., 2018. PEDOT:PSS-based Multilayer Bacterial-Composite Films for Bioelectronics.
453 Sci. Rep. 8, 15293. https://doi.org/10.1038/s41598-018-33521-9
454 Zheng, X.-M., Hong, J., Li, H.-Y., Lin, D.-H., Hu, H.-Y., 2012. Biochemical properties and catalytic
455 domain structure of the CcmH protein from Escherichia coli. Biochim. Biophys. Acta 1824, 1394–
456 1400. https://doi.org/10.1016/j.bbapap.2012.06.017
457 Zhou, A.Y., Baruch, M., Ajo-Franklin, C.M., Maharbiz, M.M., 2017. A portable bioelectronic sensing
458 system (BESSY) for environmental deployment incorporating differential microbial sensing in
459 miniaturized reactors. PLoS One 12, e0184994. https://doi.org/10.1371/journal.pone.0184994

460 **FIGURE CAPTIONS**

461 **Figure 1. A schematic illustration depicting the different *ccmH* genes for cytochrome *c***
462 **expression in engineered *E. coli*.** We replaced the coding sequence of *ccmH* from the *E. coli*
463 *ccmABCDEFGH* operon with three other variants. These variants coded for CcmHI from MR-1
464 (*ccmHI*), a fusion between the N terminal region of *E. coli ccmH* and the C terminal region of
465 CcmI from MR-1 (hybrid *ccmH*), and a control that removed the C terminal region of MR-1 CcmI
466 *(ccmH^N)*. Black and red regions indicate DNA regions that code for proteins from *E. coli* and MR-
467 1, respectively.

468 **Figure 2. The hybrid *ccmH* strain expresses more cytochromes *c*.** Relative redness as a function
469 of relative promoter strength, i.e., induction level, for *E. coli* expressing *cymAmtrCAB* with
470 different *ccm* operons. The hybrid *ccmH* strain has a higher level of overall cyt *c* expression than
471 wildtype *ccm*. Results are representative of three independent experiments.

472 **Figure 3. The hybrid *ccm* system increases the CymA expression in *E. coli*.** The relative density
473 of enhanced chemiluminescence (ECL) bands arising from three cyt *c* heterologously expressed
474 in the hybrid *ccm* and wildtype *ccm* strains. The cyt *c* expression in negative control no *ccm* strain
475 was below the limit of detection. Results are representative of three independent experiments.

476 **Figure 4. The hybrid *ccmH* strain produces a higher current.** The current generation measured
477 by chronoamperometry in the bioreactors showing hybrid *ccmH* strain produces more current than
478 the wildtype *ccm*, while the negative control strain *ccmH^N* produces less current. Results are
479 representative of three independent experiments. The dotted arrow shows the injecting time of
480 bacteria.

481 **Figure 5. The hybrid *ccmH* strain shows higher redox activity through cyt *c*.** Differential pulse
482 voltammetry (DPV) shows that the hybrid *ccmH* strain has a higher redox peak at the cyt *c* related
483 redox reaction potential (+51 mV vs. SHE). DPV signal smoothing and background deduction by
484 QSoas Version 2.0 (Fourmond et al., 2009).

485 **Figure 6. Current production by the hybrid *ccmH* strain is more sensitive to exogenous**
486 **flavins.** (A) The hybrid *ccmH* strain (red) has a more rapid and higher current response as a
487 function of extra riboflavin concentration, compared to the wildtype *ccm* strain (gray), and $ccmH^N$
488 strain (yellow). Results are representative of two independent experiments. Linear fit analysis
489 (with Y error) is performed by OriginPro 2019b (OriginLab Corporation). (B) A schematic
490 depicting the extracellular electron transfer via Mtr conduit. MtrCAB complex receives the
491 electrons from CymA (I_{strain}), then delivers to the electrode through either MtrC (I_{Mtr}) or flavin
492 (I_{flavin}). (OM: outer membranes, IM: Inner membranes).

Figure1

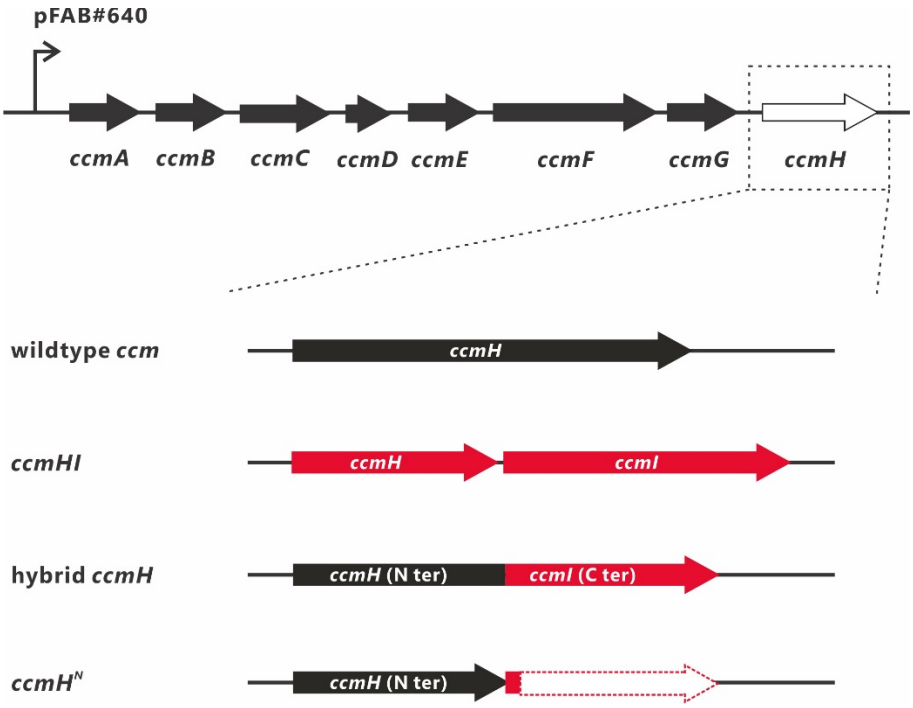
pFAB#640
ccmA
ccmB
ccmC
ccmD
ccmE
ccmF
ccmG
ccmH
wildtype ccm
ccmH
ccmHI
ccmH
ccmI
hybrid ccmH
ccmH (N ter)
ccmI (C ter)
ccmH^N
ccmH (N ter)

Figure2

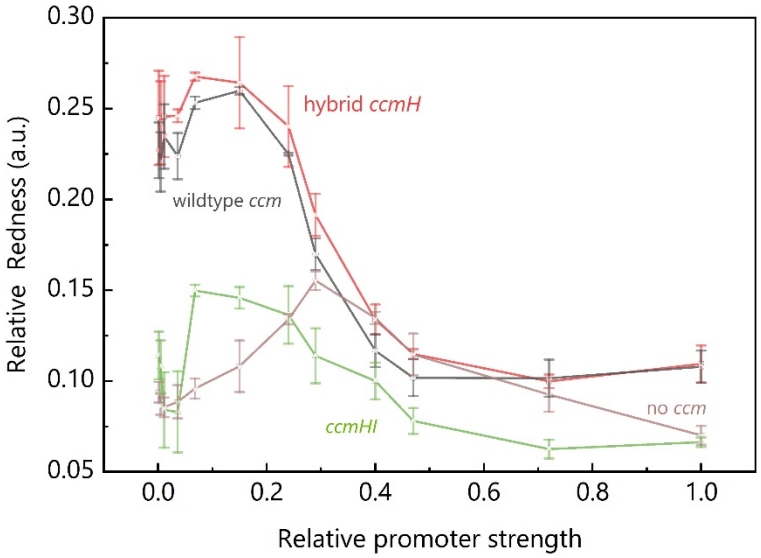
0.30
0.25
0.20
0.15
0.10
0.05
Relative Redness (a.u.)
0.0
0.2
0.4
0.6
0.8
1.0
Relative promoter strength
hybrid ccmH
wildtype ccm
no ccm
ccmHI

Figure3

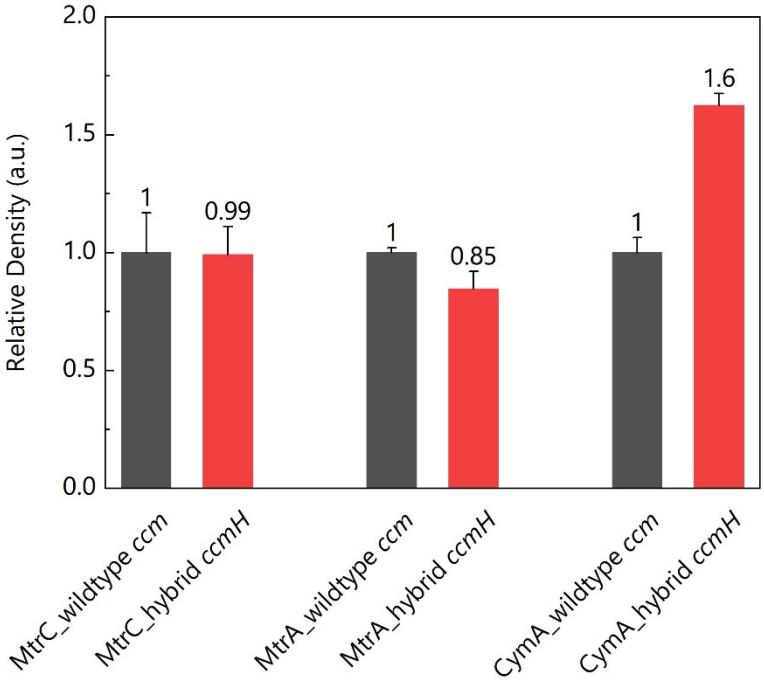
2.0
1.5
1.0
0.5
0.0
Relative Density (a.u.)
1
0.99
1
0.85
1
1.6
MtrC_wildtype ccm
MtrC_hybrid ccmH
MtrA_wildtype ccm
MtrA_hybrid ccmH
CymA_wildtype ccm
CymA_hybrid ccmH

Figure4

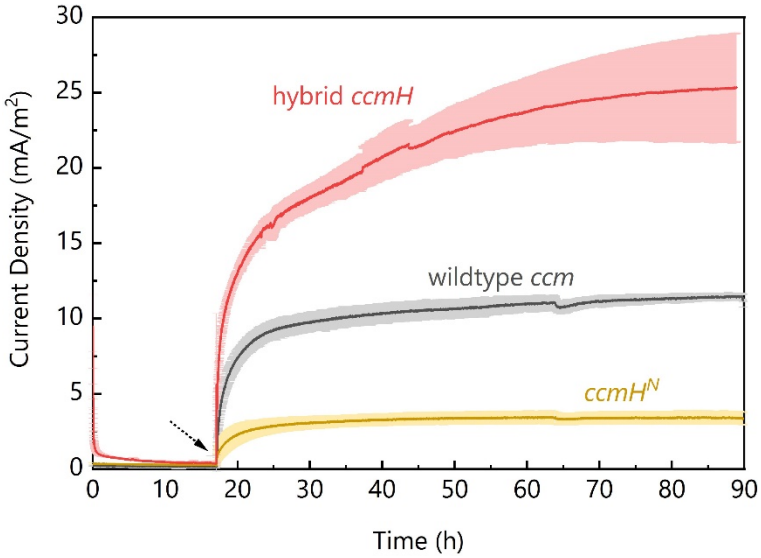
hybrid *ccmH*
wildtype *ccm*
ccmH^{N}
Current Density (mA/m^2)
Time (h)
0
5
10
15
20
25
30
0
10
20
30
40
50
60
70
80
90

Figure5

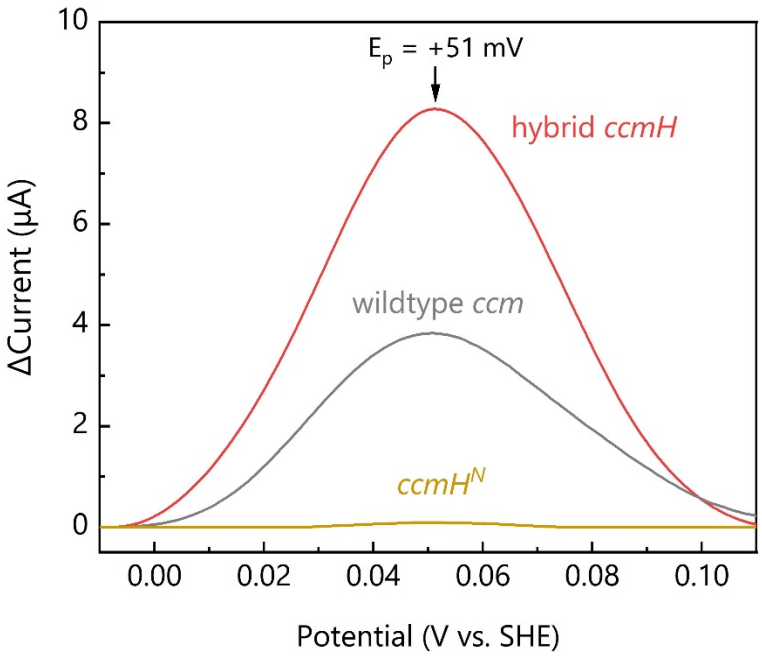
10
8
6
4
2
0
ΔCurrent (μA)
0.00
0.02
0.04
0.06
0.08
0.10
Potential (V vs. SHE)
Ep = +51 mV
hybrid ccmH
wildtype ccm
ccmHN

Figure6

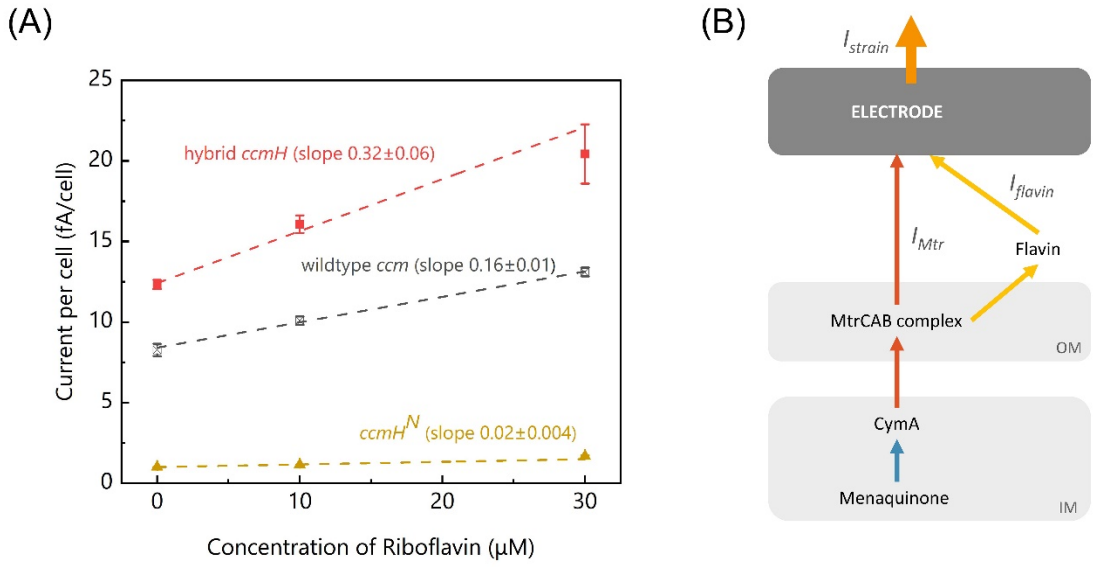
(A)
hybrid ccmH (slope 0.32±0.06)
wildtype ccm (slope 0.16±0.01)
ccmH^N (slope 0.02±0.004)
Current per cell (fA/cell)
Concentration of Riboflavin (μM)
0
5
10
15
20
25
0
10
20
30
(B)
I strain
ELECTRODE
I flavin
I Mtr
Flavin
MtrCAB complex
OM
CymA
Menaquinone
IM